Received 1 October 2019; revised 19 November 2019; accepted 20 November 2019.
Date of publication 25 November 2019; date of current version 2 January 2020.

Digital Object Identifier 10.1109/OJAP.2019.2955507

Screen-Printed, Flexible, Parasitic Beam-Switching Millimeter-Wave Antenna Array for Wearable Applications

AZAT MEREDOV[1,2], KIRILL KLIONOVSKI[1], AND ATIF SHAMIM[1] (Senior Member, IEEE)

[1] Computer, Electrical and Mathematical Sciences and Engineering Division, King Abdullah University of Science and Technology, Thuwal 23955-6900, Saudi Arabia
[2] Department of Electrical Engineering, RWTH Aachen University, 52056 Aachen, Germany

CORRESPONDING AUTHOR: K. KLIONOVSKI (e-mail: kirill.klionovski@kaust.edu.sa)

ABSTRACT Millimeter wave antennas have applications in several sensing and communication systems. Such antennas, designed for modern miniaturized devices and systems, must be low profile, flexible, and low cost. Some applications also require beam steering for detection purposes. Combining all these features into an antenna system and delivering decent antenna performance is challenging. In this study, we combined a partially reflective surface with a parasitic patch array to create a simple beam-switching, low-profile, and flexible wearable detection system. To ensure lower costs as well as compatibility with wearable systems, screen printing was utilized on a flexible substrate. The antenna array was optimized for the 77 GHz band and had a high gain of 11.2 dBi. The designed system has three independent beams, which can be oriented from bore-sight to $\pm 32^{\circ}$ through a simple switching mechanism. The antenna array maintains its performance in both flat and flexed conditions. Finally, the antenna array was tested in the field to successfully detect objects moving in three different directions.

INDEX TERMS Additive manufacturing, beam switching, flexible, low-profile antenna, mm-wave antenna, partially reflecting surface, parasitic antenna arrays.

I. INTRODUCTION

MILLIMETER (mm)-wave antennas are required for a wide range of applications, such as 5G communication, radio frequency (RF) identification, automotive radars, and more. Object detection or sensing through electromagnetic waves is also becoming popular for wearable applications. One possible application for such wearable sensing systems is to provide assistance to visually impaired people when walking [1]. Such antennas require either multidirectional beams or certain types of beam switching or steering. In addition, they require a low profile to ensure they can be easily embedded in modern miniature designs. Flexibility is also desirable for wearable applications. Finally, lower cost is a consideration for almost all wearable applications. However, designing a beam-steerable antenna system that is low-cost, low-profile, and flexible with a simple beam-steering mechanism and decent performance (i.e., gain, efficiency, and beamwidth) is quite challenging.

Continuous beam steering can be achieved using techniques such as mechanical scanning, electrical scanning (e.g., phase shifters), and frequency scanning. Mechanical scanning requires bulky components, which makes it infeasible for modern miniature designs. Furthermore, utilizing discrete phase shifters at each element for mm-wave frequencies would make the antenna array expensive, narrow-banded, and lossy.

By contrast, beam switching (i.e., beam steering at discrete points) offers a comparatively simpler approach. Beam switching may be achieved using Butler and Blass matrices, a Rotman lens, or parasitic antenna arrays. However, couplers, crossovers, and delay lines in the Butler matrix add extra power losses to the system. Similarly, Rotman lenses are unsuitable for wearable applications because of their significantly large dimensions. Moreover, parasitic antenna arrays exhibit potential for low-loss and flexible beam-switching systems.

TABLE 1. Comparison of parasitic antenna arrays.

Paper	Antenna type	Central frequency, GHz	Gain, dBi	Beam switching range, degree	Bandwidth, %	Flexible	Additive Manufacturing
[2]	Parasitic patch antenna array	1.5	2.6	±20	2	No	No
[3]	Parasitic monopole antenna array	1.5	-	90	-	No	No
[4]	Parasitic patch antenna array	2.4	8.2	±15	1.5	No	No
[5]	Parasitic patch antenna array	5.8	7.5	±50	3.5	No	No
[6]	Parasitic monopole antenna array	2.4	5.9	90	8	No	No
This work	Parasitic patch antenna array with PRS	77	11.2	±32	5	Yes	Yes

A parasitic antenna array directs the antenna beam using parasitic elements that are close to a driven (i.e., directly fed) antenna. Current is induced into the parasitic elements through mutual coupling from the main driven antenna. The radiation from these parasitic elements changes the total radiation pattern of the array. A parasitic antenna array has only one driven element, which helps to avoid distribution network losses. Some designs of various parasitic antenna arrays have been presented in [2]–[6]. In [2], a patch antenna array with parasitic patches was employed to track polar-orbiting satellites. Beam switching through a parasitic monopole antenna array was utilized in [3] to determine the direction of the nearest base station. An array of four parasitic circular patches was used in [4] to switch the beam in four different directions for a WiMAX application. Finally, a wide switching range was demonstrated in [5], which utilized parasitic antenna elements. Paper [6] describes a design of a parasitic monopole antenna array. Although the parasitic antenna array-based beam-switching mechanism is simpler and has lower loss, it has the disadvantages of a wide beamwidth and lower directivity. Furthermore, unlike conventional antenna arrays with a feed network, the beamwidth does not become narrower when the number of array elements is increased. Because narrow beams are desirable for increasing detectability in most beam steering and switching applications, design techniques must be adapted to narrow the beam for parasitic arrays.

Typically, narrow beams (enhanced directivity) can be achieved through lenses, reflectors, or transmit arrays. However, these methods are generally unsuitable for low-profile, flexible, and planar designs. An alternate approach is a partially reflective surface (PRS), which can be realized on top of the antenna through a thin flexible superstrate layer. Studies have demonstrated multiple antennas with a PRS layer [7]–[15]. However, the concept of PRS has never been applied to enhance the directivity of a parasitic antenna array or flexible antennas.

This paper presents a beam-switching parasitic antenna array that is loaded with a PRS. Because of these design choices (i.e., a parasitic array and PRS), the antenna system is low profile. It was realized on a flexible substrate to enhance its suitability for wearable applications. The antenna was developed through screen printing to make it cost-effective. Table 1 compares our work with the published parasitic antenna arrays. It indicates that our antenna array is the only one that is flexible and was realized through additive manufacturing technique. The antenna has a ±32° beam-switching range, which is said to be the limit of the parasitic antenna array concept. This limit can be further extended up to 50° using the ground-plane truncation method described in [5]. This method was not employed in the present study because of the fabrication limitations of a W-band antenna dues to its small dimensions. To the authors' knowledge, the presented antenna array has the highest gain among the published parasitic patch array designs (11.2 dBi) as a result of PRS integration. Furthermore, it is apparent that we have one of the lowest profiles and a comparable gain with other published PRS antennas. The low profile, flexibility, narrow beamwidth (i.e., high directivity), simple beam-switching mechanism, and low cost are features of the proposed design that are attractive for various wearable sensing applications.

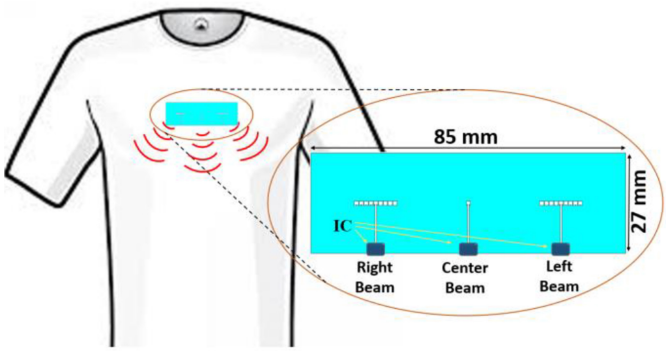

FIGURE 1. Intended antenna design with three beams on a t-shirt for a sensing application.

II. ANTENNA DESIGN

The objective of this study was to demonstrate a low-profile, flexible, simple beam-switching antenna for wearable applications. Because most detectors (radars) utilize the 77 GHz band, it was chosen as the center frequency of the antenna system in this study. The antenna was designed on a low-loss (loss tangent = 0.0044) flexible substrate from PremixGroup with a permittivity of 2.6 [16]. Antenna simulations were performed using CST Microwave Studio.

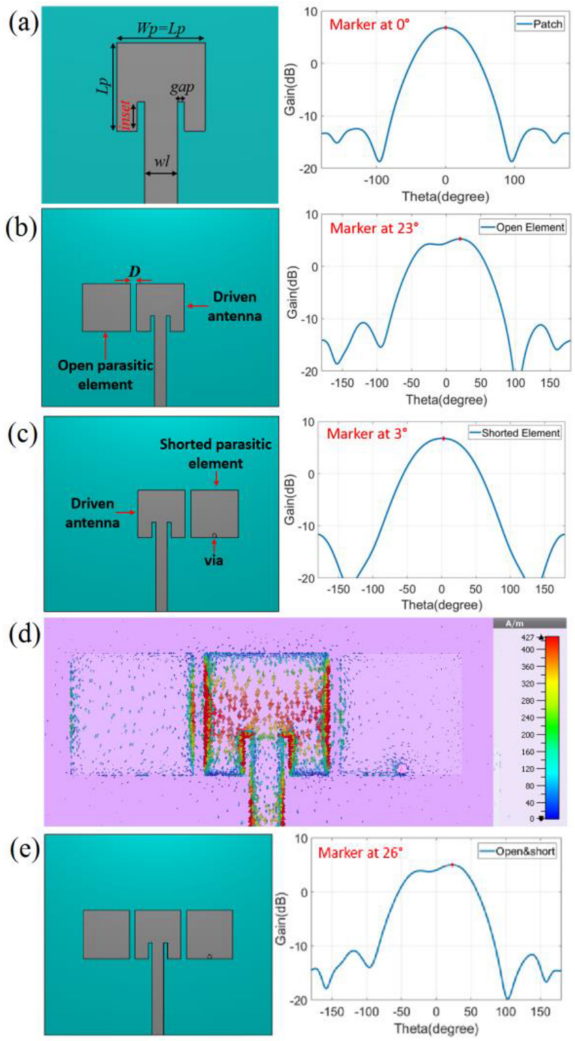

FIGURE 2. (a) Single element patch antenna and H-plane radiation pattern; (b) parasitic array with an open parasitic element and its H-plane radiation pattern; (c) parasitic array with a shorted parasitic element and its H-plane radiation pattern; (d) surface current plot; (e) parasitic patch array with an open and a short parasitic element and its H-plane radiation pattern.

As a proof of concept, we designed a wearable antenna to detect obstacles in three directions (i.e., slightly right, front, and slightly left). This is intended to be a wearable device and can be attached to the chest area, as shown in Fig. 1. Each antenna is connected to a separate integrated circuit (IC) to provide a continuous operating mode for each beam. Fig. 1 depicts these three antennas with dedicated ICs for three directions. The antennas occupy a square measuring 85 mm $\times$ 27 mm on the textile.

A. MICROSTRIP PATCH ANTENNA

A microstrip patch antenna was chosen because it has a ground plane that can shield the antenna from the losses of the human body. Because a single patch antenna has a bore-sight maximum radiation pattern, it can be used to realize the central beam, whereas the left- and right-tilted beams can be created through parasitic antenna arrays with one driven

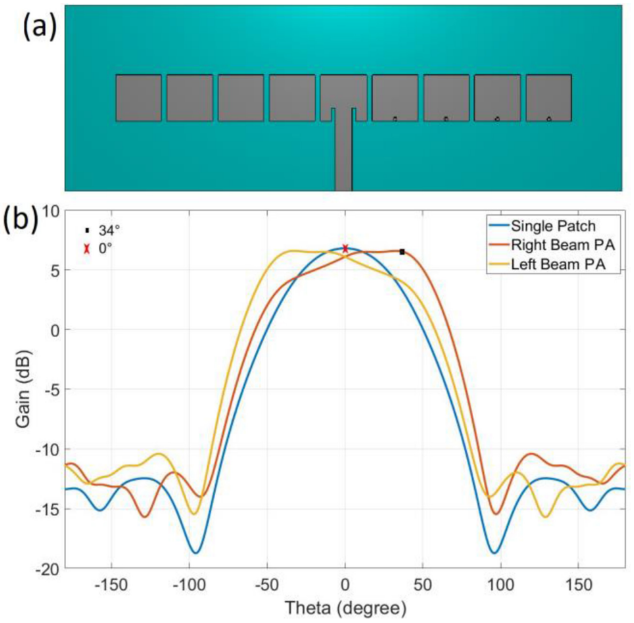

FIGURE 3. (a) Parasitic antenna array (PA) with eight parasitic elements; (b) H-Plane radiation patterns of a single active element and parasitic antenna array.

element in each (discussed in detail in the following subsection). The single-patch antenna was fed through a 50 Ω microstrip line with inset feeding (Fig. 2(a)); it had a gain of 6.8 dBi and a half-power beamwidth (HPBW) of 68°.

B. PARASITIC ANTENNA ARRAY

As explained in the Introduction section, parasitic antennas can be used for tilting the beam. Fig. 2(b) clearly shows that the bore-sight maximum beam of the single patch antenna can be tilted to the right side (23° from the bore-sight) by adding an open (i.e., not connected to any metal) parasitic element next to it (on the left side). Furthermore, the maximum beam can be slightly tilted (by only a few degrees) to the right by adding a shorted (i.e., connected to the ground through a metalized via) parasitic element on the right side of the driven element (Fig. 2(c)). The antenna surface current plot in Fig. 2(d) shows that the open parasitic element has a stronger coupling compared with the shorted parasitic element. Thus, the open parasitic element has more of an effect on the radiation pattern of the parasitic array. Combining both the abovementioned cases, the maximum angle of the parasitic array switches to 26° when open and shorted parasitic elements are placed next to the driven element, as shown in Fig. 2(e). The number of the parasitic elements was increased to four on each side of the driven patch to tilt the maximum beam angle to 34°, as shown in Fig. 3a. This study observed that the further increase in the number of parasitic elements did not increase the maximum beam angle (due to weaker coupling in the farthest parasitic elements). Thus, in this study, a parasitic antenna array with eight parasitic elements (four open and four shorted) was designed that demonstrated a gain of 6.59 dBi and an

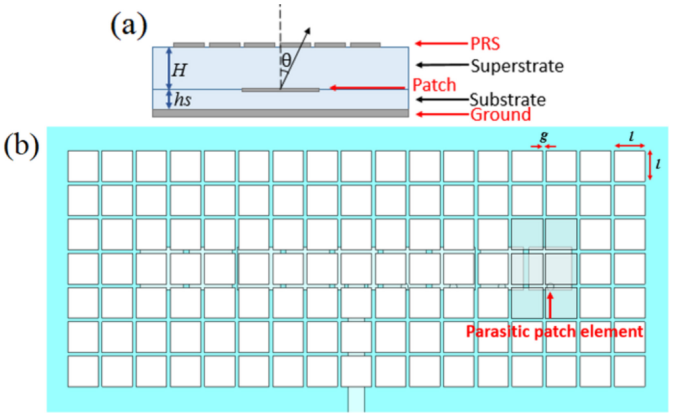

FIGURE 4. (a) Antenna stack up; (b) parasitic patch array with PRS (top view).

TABLE 2. Antenna dimensions.

	Single Patch (mm)	Parasitic Antenna Array (mm)
Substrate thickness (***hs***)	0.15	0.15
Square patch length (***Lp***)	1.13	1.15
Inset length (***inset***)	0.3	0.3
Feed line width (***wl***)	0.45	0.45
Inset Gap (***gap***)	0.1	0.1
Distance between patches (***D***)	-	0.15
Superstrate thickness (***H***)	1.3	1.3
PRS patch size (***l***)	0.75	0.85
Spacing between PRS cells (***g***)	0.1	0.1
Number of PRS units	9×9	15×15
Ground plane	20×20	35×20
Substrate dimensions	20×27	35×27
Size of metal sheet (***a***)	-	16

HPBW of 96.9° (Fig. 3b). A beam with a maximum of −34° was obtained by interchanging the open parasitic elements with the shorted ones. As Fig. 3(b) indicates, the antenna array beamwidth was quite wide and unsuitable for detecting objects uniquely. To effectively distinguish signals from three directions, we had to decrease the beamwidth of both the single element patch and parasitic antenna arrays. A PRS structure on top of the antenna array can be beneficial for achieving a narrower beam.

C. PRS

The operational principle of the PRS layer is that an electromagnetic wave that travels through the layer is partially reflected and then partially transmitted through the surface. By changing the reflection and transmission properties of the PRS, we could obtain co-phase radiation of a transmitted wave and a wave reflected from the ground plane of the antenna (Fig. 4). Co-phase radiation allowed us to increase the gain and make the beamwidth narrower. To obtain co-phase radiation, a matrix of periodically placed small square patches with side length l and gap g was placed on top of a superstrate layer of PreFlex material with thickness H. We assumed that the PRS for plane wave excitation with an incident angle θ is characterized by the reflection coefficient of $R(\theta)e^{j\varphi(\theta)}$. Then, the total radiation pattern of the patch antenna with PRS could be found through the following analytical formula [7]:

$$F^{PRS}(\theta) = \frac{\left\{1 - R(\theta)^2\right\} f(\theta)}{1 + R(\theta)^2 - 2R(\theta)\cos(\alpha(\theta))}, \quad (1)$$

$$\alpha(\theta) = \varphi(\theta) - \pi - \frac{4\pi\sqrt{\varepsilon_r}}{\lambda}(H + hs)\cos(\theta), \quad (2)$$

where $f(\theta)$, λ, and ε_r are the pattern of the source antenna, wavelength, and permittivity of the superstrate, respectively. When $\alpha(\theta_0) = 0$, we had maximum directivity

$$D_{\max} = \frac{1 + R(\theta_0)}{1 - R(\theta_0)}, \quad (3)$$

for a certain angle θ_0. In our case, the goal was to maximize the directivity for angles $\theta_0 = 0°$ and $\theta_0 = 30°$ for a single patch and parasitic antenna array, respectively. Therefore, $\alpha(\theta_0) = 0$ had to be satisfied for the required angles. When (2) was equal to zero, we obtained the following condition for the phase of the reflection coefficient:

$$\varphi(\theta_0) = \pi + \frac{4\pi\sqrt{\varepsilon_r}}{\lambda}(H + hs)\cos(\theta_o). \quad (4)$$

For the given H and hs (1.3 and 0.15 mm, respectively), we calculated the $\varphi(\theta_0)$ (phase of the PRS reflection coefficient). For $\theta_0 = 0$, the calculated φ value was $-105°$, and φ was -152 for $\theta_0 = 30°$. The parameters l and g (shown in Fig. 4 (b)) were then varied in the simulations to obtain the calculated reflection phase for the given θ_0. For the plane wave incident perpendicular to the PRS, values of $l = 0.75$ mm and $g = 0.1$ mm resulted in a $-105°$ reflection phase. These l and g values gave the highest directivity for the single patch antenna. The PRS with the determined l and g values was then placed on top of the parasitic antenna, and the values of l and g were optimized to achieve the highest gain (considering the screen printing minimum feature limitations). The optimal parasitic antenna performance was obtained when $l = 0.85$ mm and $g = 0.1$ mm.

Table 2 specifies the final dimensions of the single patch antenna and the parasitic antenna array integrated with the PRS. In our simulations, we employed a lossy conductor with a conductivity of 10^7 S/m, which is the measured conductivity of the stretchable silver ink used in our fabrication.

Fig. 5 presents the H-plane radiation patterns of the single-patch antenna and parasitic antenna array with PRS. The figure illustrates that the single antenna with the PRS had a gain of 13 dBi and HPBW of 28.5°, and the parasitic antenna array had a gain of 10.8 dBi and HPBW of 15.8°. Both antennas exhibited an HPBW of approximately 30° in the E-plane. The gain of the antennas with PRS increased by more than 4 dB. Furthermore, we noted an 8-dB side-lobe level (SLL) for the parasitic antenna array with PRS.

To decrease the SLL, the left half of the PRS structure on top of the parasitic antenna array in Fig. 4(b) was replaced with a square metal sheet with a length a (Fig. 6(a)). The

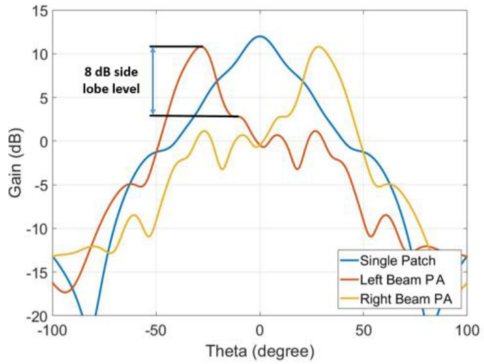

FIGURE 5. H-plane radiation pattern of the single element and parasitic patch with PRS.

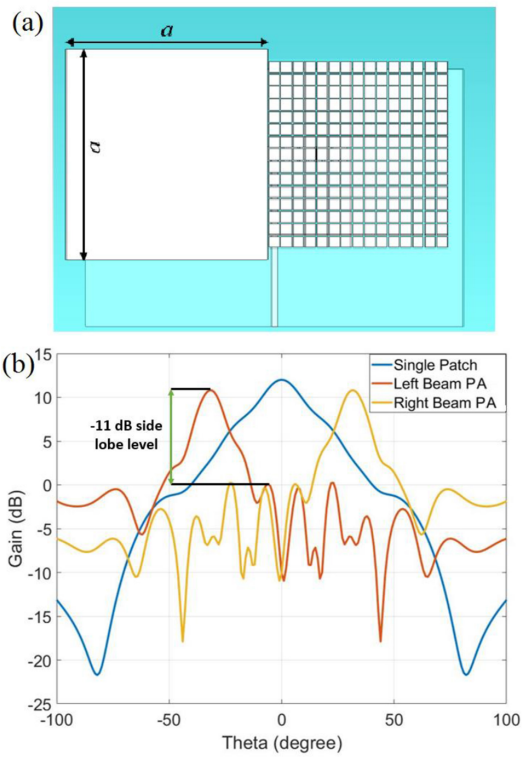

FIGURE 6. (a) Parasitic antenna array with PRS and metal sheet; (b) H-plane radiation pattern of the single-patch and parasitic antenna array with updated PRS.

dimensions of the metallic sheet were chosen to be almost similar to the PRS (slightly larger) for optimal performance. With the help of the metal sheet, the SLL was increased to 11 dB (Fig. 6(b)). To study the human body effects in the vicinity, the designed antenna was simulated with a human body phantom and the results did not change. The maximum gain, maximum angle, and SLL were the same as in the presented design.

D. FLEXED ANTENNA

Wearable devices should have flexibility to assume the shape of the clothes to which they are attached. Thus, flexibility is an essential aspect of wearable electronics. We performed simulations for flexed antennas to ensure that bending would

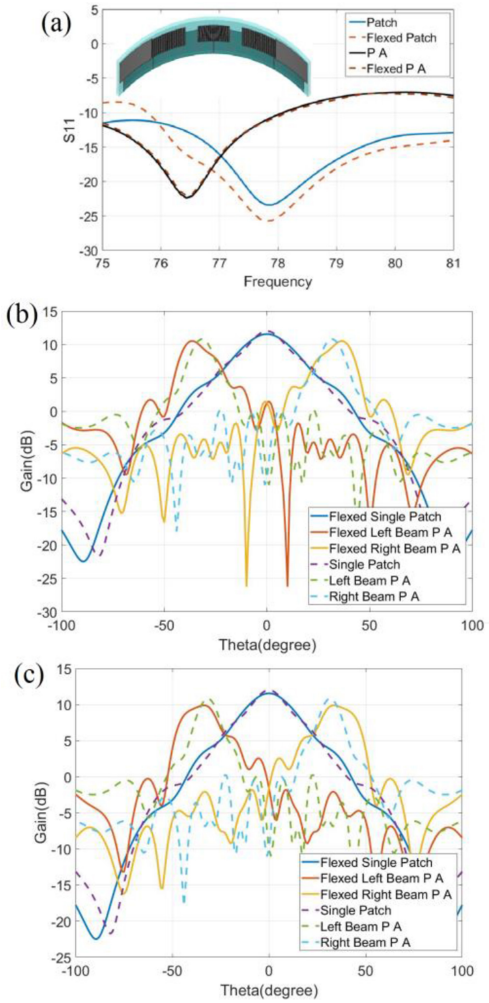

FIGURE 7. (a) S-parameters of the planar and flexed antennas with a bent antenna at the inset (R = 50 mm); (b) H-plane radiation pattern of the bent antenna with a 100-mm bend radius; (c) H-plane radiation pattern of the bent antenna with a 50-mm bend radius.

not deteriorate the antenna's performance beyond acceptable limits. For this investigation, the antenna was bent around cylinders with radii of 50 mm and 100 mm. These radii are sufficient for mounting the antenna on most common places on the human body, such as chest or even the arms. Fig. 7(a) visualizes the bending of the antenna around a cylinder with a 50-mm radius. Fig. 7(b) shows that the bending did not significantly change the return loss of the antennas in either orientation (single patch and parasitic array). Fig. 7(c) presents the bent antenna radiation pattern results, which confirm that the bending did not significantly alter the antenna radiation performance. The beamwidth of the antennas increased and the gain decreased at approximately 0.5 dB when the antenna was bent around the cylinder with a 100-mm radius, and it decreased at approximately 1 dB when it was bent around the cylinder with a 50-mm radius; however, the three beams were still quite distinguishable. The side lobe levels of the bent antennas were approximately 8 dB, which is still in the acceptable level.

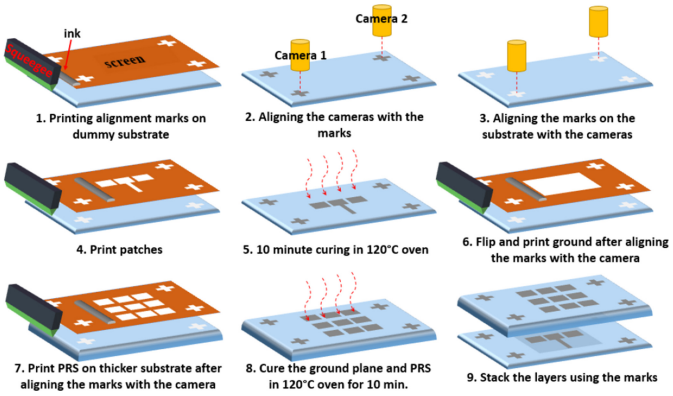

FIGURE 8. The fabrication process.

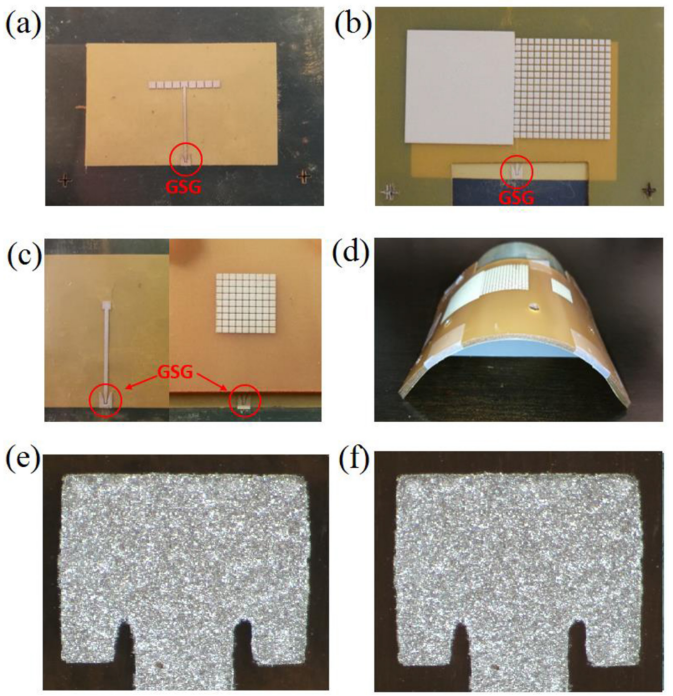

FIGURE 9. (a) Parasitic antenna array; (b) PRS for the parasitic antenna array; (c) patch antenna and its PRS layer; (d) bent antenna with a 50-mm bend radius; (e) patch antenna image under microscope for the non-bent case; and (f) patch antenna image under microscope for the bent case.

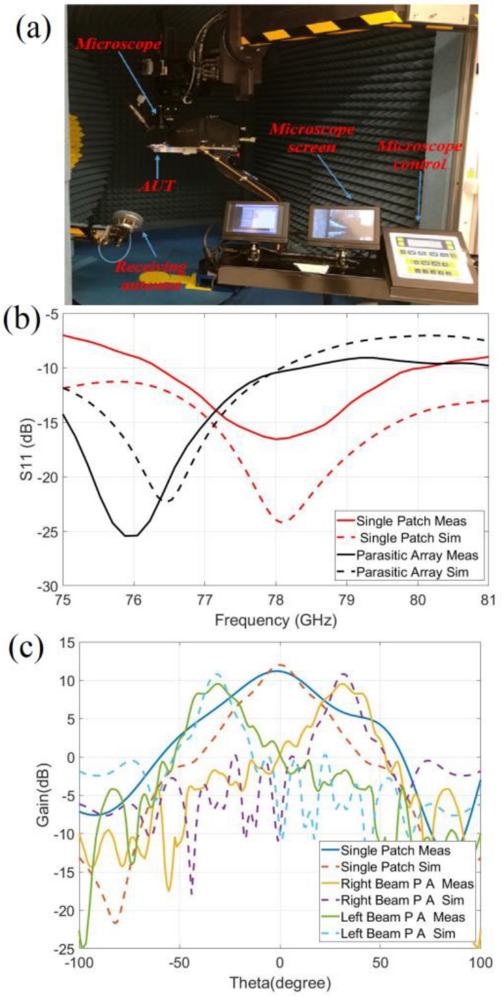

FIGURE 10. (a) Measurement of the antenna inside the anechoic chamber; (b) comparison of simulated (Sim) and measured (Meas) return losses of the single-patch antenna with PRS and parasitic antenna array with PRS; (c) H-plane radiation patterns of the single-patch antenna with PRS and parasitic antenna array with PRS.

III. FABRICATION AND MEASUREMENTS

The antennas were realized through a screen-printing (Aurel Automation 900 screen printer) process. Figs. 8 and 9 show the fabrication process and the fabricated antennas, respectively. To this end, a screen for the designed antenna was prepared. Cross-shaped alignment marks were added to align the antenna layers and shorting vias for the parasitic antenna array. The crosses for alignment were printed on a dummy substrate, and two printer cameras were manually aligned with them. A 2.5% diluted stretchable silver ink DuPont PE873 [17] was used to screen print our antenna on the low-loss flexible material. The stretchability of the ink was studied in [18], where it is shown that the ink can be stretched by 25%. First, the antenna was printed on the substrate according to the alignment marks and the cameras were aligned with these marks. Four shorting vias were generated by manually applying ink on the holes that were formed by a laser. Then, the substrate was flipped, and the ground layer was printed after being aligned with the marks. Lastly, the superstrate layer was printed on a different substrate (the same material as the antenna substrate) but with a larger thickness. After each layer of printing, the printed ink was cured in an oven at 120°C for 10 minutes. The measured ink conductivity after curing is $2\text{x}10^6$ S/m. The thickness of the printed conductive layer is 2.5 μm. All printed layers were stacked through the use of extra alignment marks. The air gap between the antenna layers was removed by adding plastic screws on multiple points around the antenna. Notably, we did not use glue because its dielectric properties at high frequencies are unknown and could affect the antenna's performance. Because of the lack of coaxial connectors that work at 77 GHz, the antennas had to be tested

TABLE 3. Simulated and measured results.

	Simulated	Measured
Gain of the single patch with PRS	12 dBi	11.2 dBi
Gain of the parasitic array with PRS	10.8 dBi	9.7 dBi
Gain of the bent single patch with PRS*	12 dBi	-
Gain of the bent parasitic array with PRS*	10.4 dBi	-
HPBW of the single patch with PRS	23°	35°
HPBW of the parasitic array with PRS	14°	22°
SLL of the parasitic array with PRS	11 dB	9 dB

* The gain could not be measured under the bent conditions as the antenna has to be tested through a GSG probe, which is very difficult to land on a bent surface.

at this frequency using ground signal ground (GSG) probes. A coplanar waveguide (CPW) transition was added to our design in anticipation of this probing. Testing with these probes is quite challenging because they are typically associated with parasitic capacitances and radiation, which can foul the measurements. The S-parameter and radiation pattern of the antennas were measured in a specialized u-lab anechoic chamber from Orbit/FR (Fig. 10a). This chamber was equipped with a probing system and a movable microscope to properly land a probe on a sample. The microscope was removed after landing the probes and when testing the antenna parameters. Fig. 10(b) presents the measured and simulated reflection coefficients (S_{11}). It shows that the antenna resonance frequencies exhibited similar trends. A slight shift in frequency occurred for the parasitic antenna array case, which was expected because they are more sensitive to the presence of a nearby probe compared with single patch antennas. Nonetheless, the antennas were matched at the desired frequencies. Fig. 10 (c) illustrates the measured and simulated radiation patterns of the antennas, which were well-aligned. The simulated and measured gain, HPBW and SLL of the antennas are presented in Table 3. The maximum value of the measured gain of the single-patch antenna with PRS was 12 dBi at an angle of 0°, whereas that of the parasitic antenna array with PRS was 9.8 dBi at an angle of 30°. The maximum measured gain was 1 dB lower than the simulated gain, which may be because of the loss tangent variance in the dielectric material and the screen-printing metal ink. The dielectric loss in the datasheet was shown to have a variance of ±10%, and the conductivity of printed metal can vary slightly from expectations because of printing and sintering conditions. Because of the complexity of probing on bent surfaces, the bent antenna could not be characterized in this study. However, we investigated the effect of bending on the ink. Figures 9 (e) and (f) show microscopic images of the printed patch antenna for the non-bent and bent case, respectively. From these images, we can see that there are no cracks on the ink, and the bending does not affect the structure of the patch.

IV. DETECTION TESTING

The detection range and object movement detection with location prediction are two main parameters for sensing

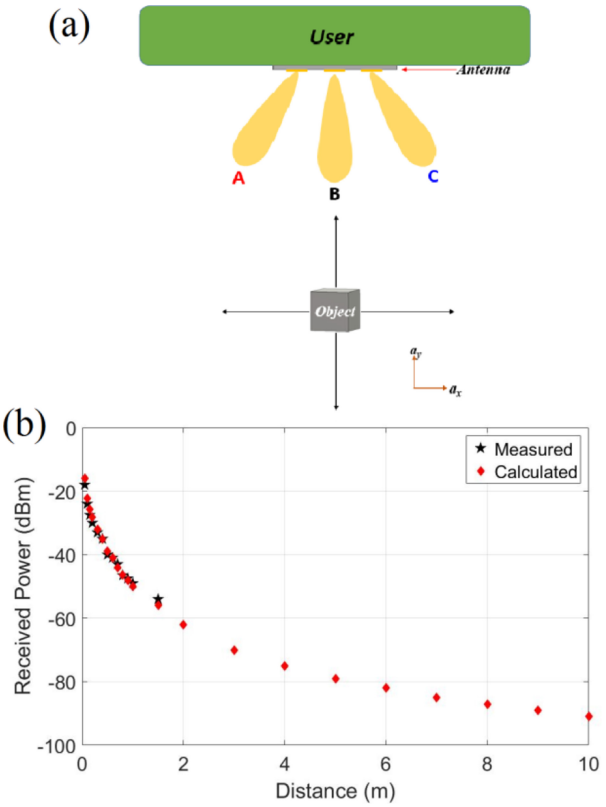

FIGURE 11. (a) Radar test method; (b) measured and calculated received power versus distance.

applications. To test them, we prepared a setup similar to that shown in Fig. 11(a), where the user is shown to have three wearable antennas (labelled A, B, and C) for the three test cases. In this setup, we used these antennas as transmit antennas and the RF input signal was provided to them using a signal generator. We used metal sheets (metalized A4 size FR-4 boards and some metal objects such as wrenches, which were present during the tests) as objects for the tests, which reflected back the transmitted signal. To receive the reflected signal, we used a spectrum analyzer that was connected to a horn antenna and placed next to the transmitting wearable antennas (A, B, and C). Because we had to test three antennas (i.e., one for each direction) with the same setup, we tested them sequentially (i.e., one at a time).

The reflected power was recorded for different distances, and the measurement results are shown in Fig. 11(b). The total loss of the cables, connectors, and mixers was 51 dBm, and due to this high loss in the test setup, the measurement range was limited. However, the sensor detection range could be calculated using the radar range equation [19]:

$$P_R = P_T G_T G_R \sigma \frac{\lambda^2}{4\pi \left(4\pi R_1^2\right)^2}, \tag{5}$$

where, P_R, P_T, σ, G_T, G_R, λ, and R_1 are received power, transmitted power, radar cross-section, gain of the transmit antenna, gain of the receive antenna, wavelength, and object distance, respectively. The calculated curve, along with the

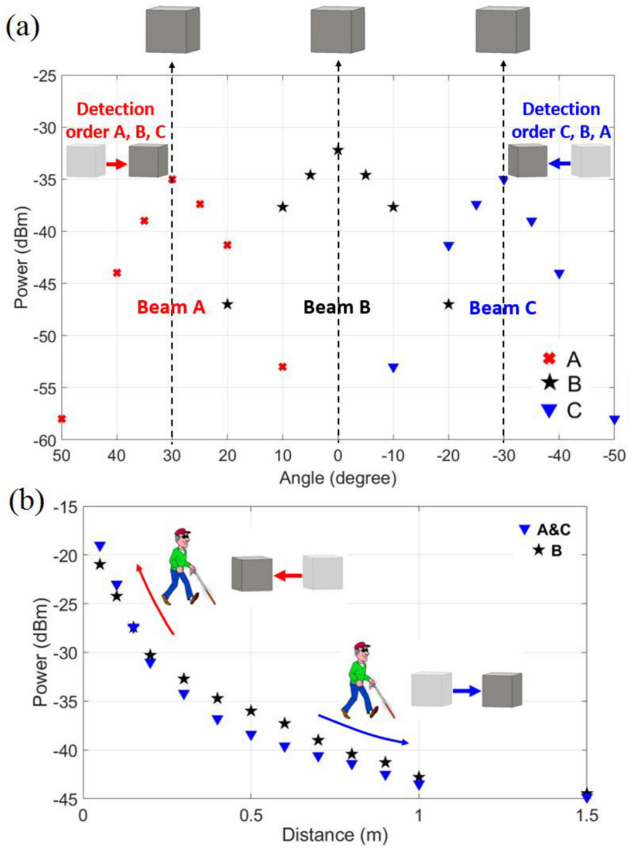

FIGURE 12. (a) Measured movement detection in the a_x direction, and (b) measured movement detection in the a_y direction. A light colored boxes has been used to show the previous position of the box (object).

measured values, is shown in Fig. 11(b). A good correlation between the measurements and calculations was observed in the initial part of the results (until approximately the 2-m range); thus, the calculated values of the remaining part of the curve can be trusted (until the 10-m range). Considering that the antennas are to be used with a power amplifier and low noise amplifier in their front ends, the received power levels will increase even more, thereby facilitating object detection beyond the 10-m range. Notably, the accurate distance and velocity of objects can be obtained by integrating the antenna with appropriate circuits to obtain the wave travel time and frequency shift. Standard signal-processing techniques can then be applied to acquire real-time information. However, this setup can also be used for a simple method to detect an object's incoming direction as well as predict the direction of its movement.

As mentioned previously, the test setup could send and receive signals from three directions with beams A (at 30°), B (at 0°), and C (at −30°). Depending on which antenna receives the maximum reflected signal, the angle of the object can be determined. For example, if the maximum reflected power is received by antenna A, the object is at 30°, whereas if the maximum is received by antenna C, the object is at −30°. Antenna B will receive maximum reflected power for 0°. Similarly, the movement direction of the object can be determined; for example, if the movement is in the $\pm a_x$ direction (according to the coordinates shown in Fig. 11(a)), the direction of movement can be determined through recording the reflected powers while the object (a metal sheet in this case) is moved in the $\pm a_x$ direction. Fig. 12(a) displays the measured results for these tests. If the object was moving in the $+a_x$ direction (right side), antenna A or B received the reflected signal first and then antenna C received it. The order of receiving the reflected signal was the opposite when the object moved in the $-a_x$ direction. This can be seen in the points measured by the three antennas in Fig. 12(a). Similarly, the movement in the $\pm a_y$ direction could be determined by moving the object in the $\pm a_y$ direction and recording the reflected powers. The results for these measurements are shown in Fig. 12(b), where it can be seen that if the object is moving in the $+a_y$ direction, the reflected power level increases with this movement, whereas the response is the other way round for $-a_y$ movement. With the help of this antenna system, the user can be informed whether the object is moving to the right or left as well as whether it is moving away or coming closer.

V. CONCLUSION

This study demonstrated a wearable antenna array with three independent beams to detect objects in three directions. The flexible, low-profile, and low-cost antenna array was designed, prototyped, and tested for this study. The tests proved that the antenna array is capable of detecting objects within a range of 10 m, which can be enhanced using suitable power and low noise amplifiers. Moreover, the direction of movement of an object can be determined using a simple technique. The combination of the three antennas can detect objects in the angle range of ±32°. The design is highly suitable for futuristic wearable sensing and detection applications.

ACKNOWLEDGMENT

The authors wish to thank the PremixGroup team for their extensive support with material information. They also thank H. Zhang and Y. H. Kuo for their assistance with the antenna range testing.

REFERENCES

[1] T. Kiuru *et al.*, "Assistive device for orientation and mobility of the visually impaired based on millimeter wave radar technology—Clinical investigation results," *Cogent Eng.*, vol. 5, no. 1, 2018, Art. no. 1450322.

[2] S. L. Preston, D. V. Thiel, J. W. Lu, S. G. O'keefe, and T. S. Bird, "Electronic beam steering using switched parasitic patch elements," *Electron. Lett.*, vol. 33, no. 1, pp. 7–8, Jan. 1997.

[3] S. L. Preston, D. V. Thiel, T. A. Smith, S. G. O'Keefe, and J. W. Lu, "Base-station tracking in mobile communications using a switched parasitic antenna array," *IEEE Trans. Antennas Propag.*, vol. 46, no. 6, pp. 841–844, Jun. 1998.

[4] M. Jusoh, T. Sabapathy, M. F. Jamlos, and M. R. Kamarudin, "Reconfigurable four-parasitic-elements patch antenna for high-gain beam switching application," *IEEE Antennas Wireless Propag. Lett.*, vol. 13, pp. 79–82, 2014.

[5] T. Sabapathy, M. Jusoh, R. B. Ahmad, M. R. Kamarudin, and P. J. Soh, "A ground-plane-truncated, broadly steerable Yagi-Uda patch array antenna," *IEEE Antennas Wireless Propag. Lett.*, vol. 15, pp. 1069–1072, 2016.

[6] S.-J. Lee, W.-S. Yoon, and S.-M. Han, "Planar beam steerable parasitic array antenna system design based on the Yagi-Uda design method," *Int. J. Antennas Propag.*, vol. 2019, Mar. 2019, Art. no. 8023712.

[7] G. V. Trentini, "Partially reflecting sheet arrays," *IRE Trans. Antennas Propag.*, vol. 4, no. 4, pp. 666–671, Oct. 1956.

[8] A. Foroozesh and L. Shafai, "Investigation into the effects of the patch-type FSS superstrate on the high-gain cavity resonance antenna design," *IEEE Trans. Antennas Propag.*, vol. 58, no. 2, pp. 258–270, Feb. 2010.

[9] R. Guzmán-Quirós, J. L. Gomez-Tornero, A. R. Weily, and Y. J. Guo, "Electronically steerable 1-D Fabry-Perot leaky-wave antenna employing a tunable high impedance surface," *IEEE Trans. Antennas Propag.*, vol. 60, no. 11, pp. 5046–5055, Nov. 2012.

[10] A. Ghasemi, S. N. Burokur, A. Dhouibi, and A. de Lustrac, "High beam steering in fabry–pérot leaky-wave antennas," *IEEE Antennas Wireless Propag. Lett.*, vol. 12, pp. 261–264, 2013.

[11] T. Debogović and J. Perruisseau-Carrier, "Array-fed partially reflective surface antenna with independent scanning and beamwidth dynamic control," *IEEE Trans. Antennas Propag.*, vol. 62, no. 1, pp. 446–449, Jan. 2014.

[12] L.-Y. Ji, Y. J. Guo, P.-Y. Qin, S.-X. Gong, and R. Mittra, "A reconfigurable partially reflective surface (PRS) antenna for beam steering," *IEEE Trans. Antennas Propag.*, vol. 63, no. 6, pp. 2387–2395, Jun. 2015.

[13] H. Moghadas, M. Daneshmand, and P. Mousavi, "MEMS-tunable half phase gradient partially reflective surface for beam-shaping," *IEEE Trans. Antennas Propag.*, vol. 63, no. 1, pp. 369–373, Jan. 2015.

[14] S. X. Ta, T. H.-Y. Nguyen, K. K. Nguyen, and C. Dao-Ngoc, "Bandwidth-enhancement of circularly-polarized fabry-perot antenna using single-layer partially reflective surface," *Int. J. RF Microw. Comput.-Aided Eng.*, vol. 29, no. 8, Aug. 2019. Art. no. e21774.

[15] L.-Y. Ji, P.-Y. Qin, Y. J. Guo, S. Genovesi, H.-L. Zhu, and Y. Zong, "A reconfigurable partially reflective surface antenna with enhanced beam steering capability," in *Proc. 13th Eur. Conf. Antennas Propag. (EUCAP)*, Krakow, Poland, Apr. 2019.

[16] *PREPERM PPE260 Material*. [Online]. Available: https://www.preperm.com/

[17] (2015). *DuPont PE873 Stretchable Silver Conductor*. [Online]. Available: https://www.dupont.com/content/dam/dupont/amer/us/en/products/ei-transformation/documents/PE873.pdf

[18] S. An, A. Meredov, and A. Shamim, "Flexible, stretchable and washable filter printed directly on textile," in *Proc. 48th Eur. Microw. Conf.*, Madrid, Spain, Sep. 2018, pp. 831–834.

[19] C. A. Balanis, *Antenna Theory: Analysis and Design*. New York, NY, USA: Wiley, 1997.

AZAT MEREDOV was born in Turkmenistan, in 1991. He received the B.S. degrees in mathematics and electrical engineering and the M.S. degree in electrical engineering from Fatih University, Istanbul, Turkey, in 2012, 2013, and 2015. He is currently pursuing the Ph.D. degree in electrical engineering with RWTH Aachen University, Aachen, Germany.

From 2015 to 2019, he was a Research Assistant with the IMPACT Lab, King Abdullah University of Science and Technology, Saudi Arabia. His research interests include the designing of antennas for various applications, development of wearable radars, and investigation of additive manufacturing techniques for electronics.

KIRILL KLIONOVSKI was born in Krasnogorsk, Russia. He received the Engineer degree (Hons.) in electrical engineering from Moscow Aviation Institute, Moscow, Russia, in 2010, and the Ph.D. degree in radiophysics from the Kotel'nikov Institute of Radioengineering and Electronics, Russian Academy of Sciences, Moscow, Russia, in 2015.

His current research interest includes the beam-switching antenna arrays designing.

ATIF SHAMIM received the M.S. and Ph.D. degrees in electrical engineering from Carleton University, Canada, in 2004 and 2009 respectively. He was an NSERC Alexander Graham Bell Graduate Scholar with Carleton University from 2007 to 2009 and an NSERC Post-Doctoral Fellow with Royal Military College Canada and the King Abdullah University of Science and Technology (KAUST) from 2009 to 2010. In August 2010, he joined the Electrical Engineering Program, KAUST, where he is currently an Associate Professor and the Principal Investigator of IMPACT Lab. He was an Invited Researcher with the VTT Micro-Modules Research Center, Oulu, Finland, in 2006. He has authored/coauthored 230 international publications, is an inventor of 25 patents and has given over 50 invited talks at various international forums. His research interests are in innovative antenna designs and their integration strategies with circuits and sensors for flexible and wearable wireless sensing systems through a combination of CMOS, and additive manufacturing technologies. His research work has won Best Paper Awards at the IEEE EuWiT 2008, the IEEE IMS 2016, the IEEE MECAP 2016, and the First Prize in the IEEE IMS 2019 3MT competition and honorable mention prizes at IEEE APS 2005, IEEE IWAT 2006, IEEE IMS 2014, and IEEE IMS 2017 (3MT competition). He was given the Ottawa Centre of Research Innovation (OCRI) Researcher of the Year Award in 2008 in Canada. His work on Wireless Dosimeter won the ITAC SMC Award at Canadian Microelectronics Corporation TEXPO in 2007. He has also won numerous business-related awards, including first prize in Canada's national business plan competition and OCRI Entrepreneur of the Year Award in 2010. He serves on the editorial board for the IEEE TRANSACTIONS ON ANTENNAS AND PROPAGATION.